Materials
Views
www.MaterialsViews.com

ADVANCED
FUNCTIONAL
MATERIALS
www.afm-journal.de

FULL PAPER

Mechano- and Photochromism from Bulk to Nanoscale: Data Storage on Individual Self-Assembled Ribbons

Damiano Genovese,* Alessandro Aliprandi, Eko A. Prasetyanto, Matteo Mauro, Michael Hirtz, Harald Fuchs, Yasuhiko Fujita, Hiroshi Uji-I, Sergei Lebedkin, Manfred Kappes, and Luisa De Cola*

A Pt(II) complex, bearing an oligo-ethyleneoxide pendant, is able to self-assemble in ultralong ribbons that display mechanochromism upon nanoscale mechanical stimuli, delivered through atomic force microscopy (AFM). Such observation paves the way to fine understanding and manipulation of the mechanochromic properties of such material at the nanoscale. AFM allows quantitative assessment of nanoscale mechanochromism as arising from static pressure (piezochromism) and from shear-based mechanical stimuli (tribochromism), and to compare them with bulk pressure-dependent luminescence observed with diamond-anvil cell (DAC) technique. Confocal spectral imaging reveals that mechanochromism only takes place within short distance from the localized mechanical stimulation, which allows to design high-density information writing with AFM nanolithography applied on individual self-assembled ribbons. Each ribbon hence serves as an individual microsystem for data storage. The orange luminescence of written information displays high contrast compared to cyan native luminescence; moreover, it can be selectively excited with visible light. In addition, ribbons show photochromism, i.e., the emission spectrum changes upon exposure to light, in a similar way as upon mechanical stress. Photochromism is here conveniently used to conceal and eventually erase information previously written with nanolithography by irradiation.

Dr. D. Genovese, Dr. M. Hirtz, Prof. H. Fuchs,
Dr. S. Lebedkin, Prof. M. Kappes, Prof. L. De Cola
Karlsruhe Institute of Technology (KIT)
Institute of Nanotechnology & Karlsruhe
Nano Micro Facility (KNMF)
Hermann-von-Helmholtz-Platz 1D
Eggenstein-Leopoldshafen 76344, Germany
E-mail: damianogeno@gmail.com; decola@unistra.fr
Dr. A. Aliprandi, Dr. E. A. Prasetyanto, Dr. M. Mauro,
Prof. L. De Cola
Laboratoire de chimie et des biomatériaux
supramoléculaires
ISIS & icFRC
Université de Strasbourg & CNRS
8 allée Gaspard Monge, Strasbour 67000, France
Dr. M. Mauro
University of Strasbourg Institute for Advanced Study (USIAS)
5 allée du Général Rouvillois, Strasbourg 67083, France
Dr. Y. Fujita, Prof. H. Uji-I
KU Leuven
Department of Chemistry
Division of Molecular Imaging and Photonics
Celestijnenlaan 200G-F, Heverlee B-3001, Belgium

1. Introduction

Luminescence mechanochromism, defined as a change of emission spectrum upon mechanical stress, has recently emerged as a powerful novel tool for a variety of applications, ranging from sensing and tracking of mechanical stress to data storage and security.[1] In particular, fluorescence-based read-out has attracted large interest in data storage and encryption. Indeed, extreme miniaturization of memory units became possible owing to single molecule sensitivity and to high spatial resolution achievable with super-resolution microscopy techniques, with the potential to provide massive increase in information density and capacity.[2]

The race for miniaturization and read-out speed demands high brightness and large signal differences between two or more states. In the most desirable case, a switchable system should feature two forms both providing intense signals, clearly distinguishable from one another, and addressable independently.[3] As a consequence, an ideal mechanochromic system features high quantum yield of both "native" (N) and "mechanically stressed" (MS) forms, large differences between their emission spectra, and large differences in excitation spectra, so that each form can be selectively excited and efficiently detected. In recent years, a broad selection of Pt(II) complexes has been prepared, which display mechanochromism, and which respond to some of these requirements.[4] However, the possibility of using them in novel high-density memory materials was never explored so far. Indeed, microcrystalline mechanochromic powders can be employed for macroscopic devices,[5] but they cannot provide the microscopic homogeneity needed for a memory substrate to be employed in operations such as exposure, writing and reading of high-density data at the nanoscale level.

De Cola et al. has recently shown[6] that supramolecular weak interactions among adjacent Pt(II) complexes can be efficiently employed to self-assemble into ultralong ribbons by means of solvent-assisted growth, leading to millimeter long structures with high level of control on the intimate molecular structure, photophysical properties and aspect ratio.

Here we report that such Pt(II)-based ribbons show intense mechanochromism, and owing to their flatness and

homogeneity within tens of micrometers scale, they allow for quantitative description of their responsivity to mechanical stresses from the bulk to the nanoscale. Furthermore, we show that such mechanochromic and photochromic self-assembled ribbons can serve as homogeneous microsubstrates for data storage, encryption, and security at the nanoscale. The tip of an atomic force microscope (AFM) was used to write sub-micrometer features with high fidelity on single ribbons, which are individually used as homogeneous memory substrates. Furthermore, the information written by AFM can be hidden by means of irradiation: light can indeed reduce and eventually cancel out the luminescence contrast between written and unwritten regions of the ribbon, leading to secure erasing the mechanically written information.

2. Morphology, Photophysics, and Mechanochromism

Supramolecular weak interactions were recently found to lead the self-assembly of Pt(II) complex 1 in ultralong ribbons in which Pt···Pt interactions did not take place.[6] This finding led us to explore the possibility of triggering metallophilic interactions by applying external stimuli to a self-assembled system. The ribbons display typical length between 250 µm and 5 mm, and an approximately rectangular cross section of aspect ratio about 1:10, featuring thickness in the range of 2–5 µm and width in the range of 15–50 µm (**Figure 1**).

The ultralong ribbons are bright cyan luminescent, and they can be individually observed by naked eye with a UV lamp (**Figure 2**f). They show a featureless band in the excitation spectrum in the UV region with an onset down to 420nm, and a

structured emission band peaking at 466, 494, and 527 nm with photoluminescence quantum yield (PLQY) Φ, value of 0.20. The relatively long excited state lifetime (τ = 1.1 µs) reveals the triplet character of the emitting state. The emission profile is typical of Pt complexes in absence of Pt···Pt interactions, and can be attributed to mainly ligand centered (π–$\pi*$) transitions. The high PLQY of the ultralong ribbons compared to the poor emission of complex 1 in solution (Φ = 1%) indicates that aggregation-induced emission is taking place (native "N" form aggregation state).[6]

Upon grinding in a mortar, ribbons are crushed to a powder (hereafter referred to as mechanically stressed "MS" form, movie M1 in Supplementary Information) which displays profoundly different photophysical properties as compared to native ribbons: a broad luminescence band appears, corresponding to bright yellow–orange emission (λ_{em} = 598 nm, Φ = 0.51), shifted by 130 nm (4737 cm^{-1}) with respect to the ribbon native luminescence and displaying a shorter, multiexponential decay (intensity weighted average excited-state lifetime, τ_{av}, 514 ns). Such a broad, bathochromically shifted luminescence band is ascribed to a triplet-manifold excited state with metal-metal-to-ligand charge transfer nature, ^{3}MMLCT, due to the establishment of metal···metal interactions in the new aggregates.[7] As shown in Figure SI1 and SI2 of the Supporting Information and similarly to what previously reported in literature,[8] X-ray diffraction patterns reveal that while native ribbons are highly microcrystalline, the powder obtained after thorough grinding is largely amorphous, with size of the crystalline domains reduced by roughly two orders of magnitude from ≈1 µm to ≈20 nm upon grinding. Moreover, we observe that a broad peak centered at 2Θ = 26.6 appears in the XRD spectrum of MS, which is consistent with a distribution of Pt···Pt distances centered at d = 3.34 Å, i.e., short enough to trigger metallophilic interactions (Figure SI3, Supporting Information). Therefore, and consistently with recent literature on mechanochromism of Pt(II) complexes, we can interpret the photophysical transformations observed in native ribbons N, upon application of mechanical stress, as the breaking of long order microcrystalline domains—in which adjacent Pt atoms are too far to interact—into smaller nanocrystalline aggregates, in which adjacent Pt atoms can come closer and promote the metallophilic interactions responsible for the yellow emission of MS (sketch in Figure 2b).

Noteworthy, this emission color change can be appreciated—even for a single ribbon—by the naked eye or with a simple CCD sensor. Such sharp color contrast arises from the high quantum yields of luminescence for both—N and MS—forms, and from the large bathochromic shift from the 450–480 nm to the 600 nm region of the visible spectrum, namely the region where human eye and color CCD sensors are most sensitive, both in terms of absolute intensity and of color detection.[9] In addition, also
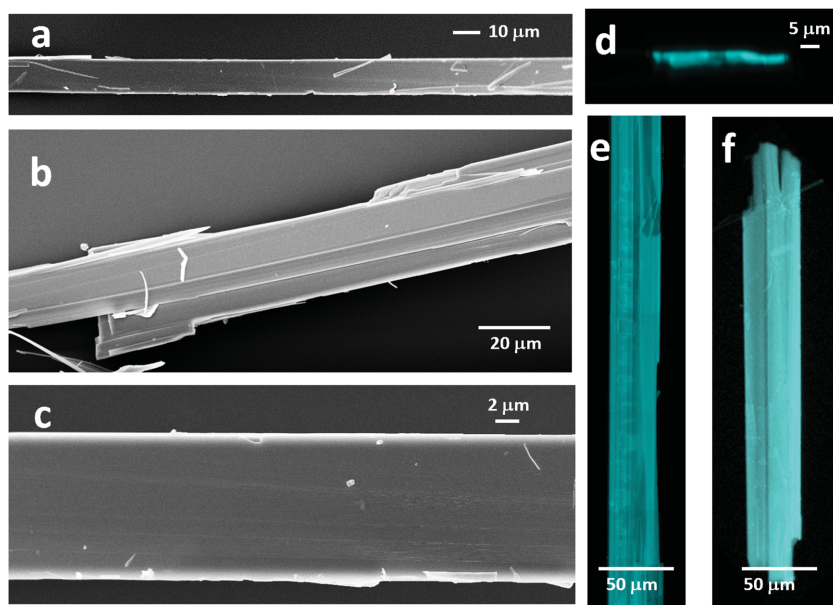

Figure 1. a–c) SEM images of ultralong ribbons at different magnifications. d) Cross-section image of a typical ribbon reconstructed by z-stacking confocal photoluminescence microscopy, showing an approximately rectangular cross section with aspect ratio of about 1:10. e,f) Confocal microscope images of typical ultralong ribbons (color coded spectral images, wavelength range 400–700 nm, λ_{exc} = 375 nm).

Materials
Views
www.MaterialsViews.com

ADVANCED
FUNCTIONAL
MATERIALS
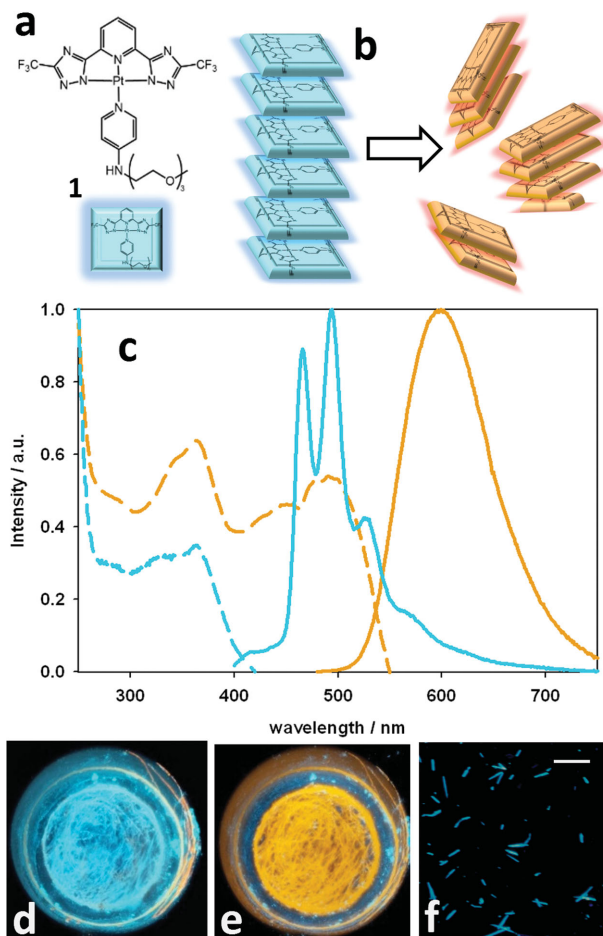www.afm-journal.de

FULL PAPER

Figure 2. a) Chemical structure of the neutral tridentate Pt(II) complex 1 and b) cartoon showing the principle of its mechanochromism, where a long crystalline domain with largely spaced adjacent Pt(II) complexes is transformed into smaller aggregates with poor crystallinity and shorter Pt···Pt distance. c) Excitation (dashed lines, λ_{emis} = 528 nm for the N and 598 nm for the MS forms) and emission spectra (solid lines, λ_{exc} = 300 nm) of the N and MS species (cyan and orange lines, respectively). Bulk mechanochromism is clearly observed upon grinding the N form with a pestle in a mortar: photographs of luminescence under top-bench UV lamp (365 nm) d) before and e) after grinding with a pestle. f) Photograph of ultralong ribbons deposited on a cover glass slide under UV lamp irradiation (λ_{exc} = 365 nm); individual ribbons are clearly visible; scale bar is 2 mm.

the excitation spectrum features important variations, in particular concerning the appearance of a new band in the region 400–550 nm. This suggests that the ground state is also significantly affected by Pt···Pt interactions, which are also responsible for the new luminescent ^{3}MMLCT state (Figure 2c). This remarkable change in the excitation spectrum is rather exceptional, since commonly observed variations are limited to band broadening.[5b,8b] This finding is of extreme importance, since the new band allows for selective excitation of the mechanically stressed material (MS form), which can thus be detected with high sensitivity.

Despite the presence in the literature of reports showing mechanochromic behavior for Pt(II) and other complexes,[4,10] quantitative information on the mechanical stresses involved

in such structural and photophysical transformations is currently largely lacking. Quantitative information is available for piezochromic and tribochromic crystals of organic molecules.[11] With the aim of reaching a quantitative description of the relationship between mechanical stresses and photophysical changes, luminescence measurements were performed versus increasing hydrostatic pressure using the diamond anvil cell (DAC) technique (see Supporting Information for further details). This technique allowed for application of uniform pressure over the whole ribbons, avoiding local phenomena such as friction and scratching or internal shear and material fracturing, none of which were observed over the explored pressure range. Emission spectra taken upon 405 nm excitation revealed that mechanochromism takes place when the applied pressure ranges between 5 and 25 kbar, with the N form spectrum disappearing while the spectrum of MS correspondingly grows (**Figure 3**). If a higher pressure is applied, we observe further bathochromic-shift of the emission spectrum which, however, is not permanent, since it returns to the MS form emission upon release of pressure. This latter, temporary bathochromic shift of the emission can be ascribed to an even closer spacing between adjacent Pt(II) centers, which can be reached when higher (>30 kbar) hydrostatic pressure is homogeneously applied to the ribbons.

Interestingly, even at high pressure it is still possible to observe the presence of some native (N) form (peaks at 466 and 494 nm) indicating only a partial conversion, while manual grinding with a mortar leads to a complete conversion from the N to the MS form (Figure 1). This observation suggests a more efficient mechanochromic response as arising from friction (tribochromism) compared to hydrostatic pressure (piezochromism). Quantitative assessment of the efficacy of friction is challenging in bulk measurements, and this motivated us to investigate the mechanochromism at the nanoscale under controlled experimental conditions.

3. Mechanochromism at the Nanoscale

The optimal morphology (flat and homogeneous on the length scale of tens of micrometers) and photophysical properties (bright contrast upon scratching) of the ultralong ribbons allowed for the first investigation of Pt(II) complexes mechanochromism at the nanoscale, with the final aim of demonstrating the applicability of these materials in high density memory and data encryption.

We used an AFM as a nanoscopic mechanical stimulation tool, whose spatial resolution is given by the effective sharpness of the tip during typical experimental procedure. The AFM is used in contact mode, generating the mechanochromic response with fine control on the applied force, on the position, and on the geometry of the system. Detection is fast and sensitive, based on photoluminescence microscopy methods: wide-field microscopy coupled to the AFM setup provides real-time monitoring of the lithography process, and confocal spectral imaging yields high-resolution spatial and spectral information. The generated mechanochromism is persistent and stable at least for months. Mechanochromism can be triggered in two different ways (sketched in **Figure 4**a), which are here

ADVANCED
FUNCTIONAL
MATERIALS
www.afm-journal.de
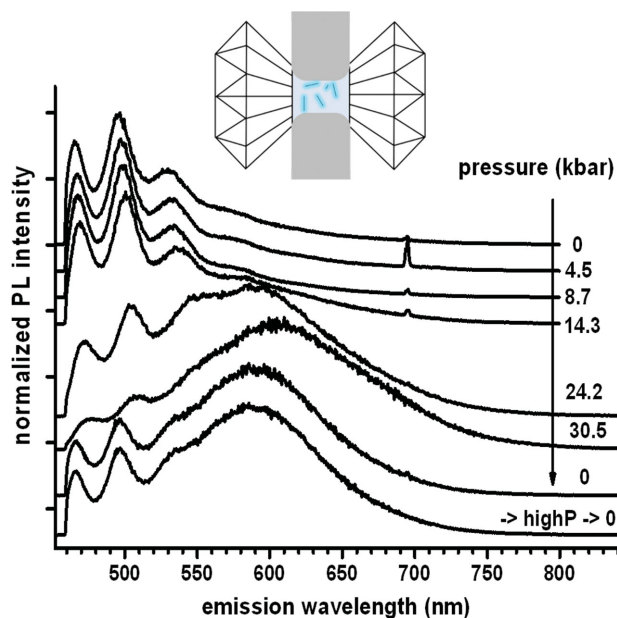
Materials Views
www.MaterialsViews.com

Figure 3. Emission spectra of Pt(II)-complex ribbons excited at 405 nm as a function of hydrostatic pressure in a diamond anvil cell (DAC, sketched in inset), two sequential cycles of pressure increase up to ≈30 kbar and pressure release. The small sharp peaks centered at 694 nm are due to weak (off-focus) emission of a ruby microcrystal.

used to modulate the mechanical stress from static pressure (piezochromism) to forces associated with high friction (tribochromism),[12] and thus to extract quantitative information on the mechanism leading to the luminescence change.

Mechanochromism is triggered by static pressure (piezochromism) when a constant force, measured after calibration of the tip, is applied locally on the ribbon by the AFM tip. Since the tip does not move in respect to the sample, static local pressure can be quantitatively estimated from the applied force and the contact area during the application of mechanical stress. Tip geometry is assessed by means of SEM directly after use of the tip: we observe different degrees of wear and of contamination

of the tip, but we can estimate an average contact surface with diameter ranging between 80 and 150 nm (see Figure SI4 of the Supporting Information). We observe first occurrence of mechanochromism at about 15 µN force (Figure 4c, white circles), which corresponds to local pressure in the range 2–7 kbar according to the actual contact area. This value is in very good agreement with quantitative information obtained with DAC technique, which showed appearance of mechanochromism in a similar pressure range. Differently from what observed in DAC experiments, when a static force larger than 40 µN (corresponding to 6–20 kbar according to the actual contact area) is applied locally with the AFM tip, fiber fracturing occurs. At such loading, the AFM tip enters deep into the fiber and originates a sudden burst of debris of scratched luminescent MS material (Figure 4i).

Mechanochromism is instead originated by friction (tribochromism) through a scanning force: if the tip is scanned over the ribbon with constant applied force, the dominating mechanical stress likely shifts from compression to shearing forces. At low scan rates (<10 µm s⁻¹) we observe a similar trend as for the simple pressure experiment, except that an earlier onset of mechanochromism can be detected, with MS emission first observed at 4 µN applied force, as well as an earlier damage of the fiber (15 µN). At high scan rates (>100 µm s⁻¹) or on particularly rough surface regions, ribbons can be heavily scratched even at very low forces (≈1 µN, data not shown), while ribbon wear and debris scattering increase due to high friction and to increased lateral forces (Figure 3c, black circles and Figure 3j).

Such results demonstrate that both tribo- and piezochromism can be triggered at the nanoscale by an AFM tip, with the friction related mechanism being more efficient than simple pressure in triggering the optical response.

It has to be noted that the emission spectrum of MS obtained with AFM stimulation is centered at 570 nm, while scratching fibers to different extents results in emission maxima ranging from 580 to 600 nm, as measured in the same confocal setup (see Figure SI5 in the Supporting Information). This indicates that at least two aggregation forms can be obtained upon controlled mechanical stimuli, corresponding to different Pt···Pt
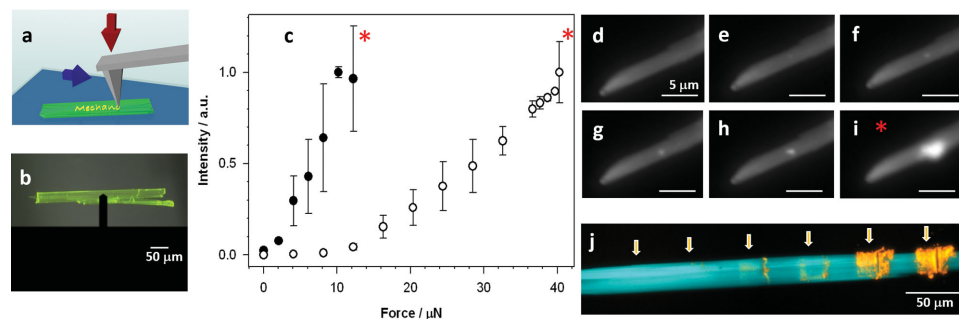

Figure 4. a) Sketch of nanomechanical stresses applied with AFM: (i) static pressure (only force perpendicular to the sample, red arrow) and (ii) shearing forces due to friction originated by scanning force (constant perpendicular force plus x–y scanning, both red and blue arrows). b) Image of AFM cantilever approaching a ribbon, overlap of photoluminescence (HC-QD filter set) and bright field images. c) Plots of MS luminescence intensity (mean values and error bars were obtained from three different experiments) during application of static force (piezochromism, white circles) or after writing squares at scan rate 10 µm s⁻¹ (tribochromism, black circles). Asterisks denote the breaking point, i.e., the force at which the ribbon is heavily damaged by the tip, resulting in sudden bursts of MS luminescence. d–i) Nanoscale piezochromism: luminescence microscopy images (FITC filter set) taken during application of static force increasing from 0 to 40 µN from panels (d) to (h), while panel (i) shows the MS luminescence burst at the breaking point. Scale-bar is 5 µm. j) Nanoscale tribochromism: confocal microscopy image of ribbon exposed to shear stress due to scanning force. Applied force is linearly increased in squares from left to right from 2 to 12 µN.

distances, which spectrally match with two metastable aggregation forms observed previously for the same complex.[6]

4. Data Storage and Photoconversion

Very importantly, no self-propagation of mechanochromism is observed along the ribbons. When an AFM tip contacts the surface and applies pressure at the contact area between tip and ribbon, mechanochromism is observed only in the very vicinity of the tip, within the resolution limit of fluorescence microscopy. Even when the tip enters deep into the material and destroys the fiber, the fracture and the consequent mechanochromism occur in a small and confined region, ascribable to the size of the whole tip cone.

This observation, together with the strong tribochromism and the dramatic change in the photoluminescent properties, led us to test the potential of the ultralong mechanochromic ribbons as memory microsystems, by using the tip of an AFM as a lithographic tool to write information on individual ribbons, following an approach similar to nanoshaving[13] or nanoscratching.[14] During the writing process, we can monitor the ribbon luminescence with UV light excitation, or visualize what is being written by selectively exciting the MS form with visible light. The information stored can indeed be read with two different excitation wavelengths: UV excitation (λ_{exc} either 355 or 405 nm) excites both N and MS forms, and provides an average vision of the emission properties of the ribbons; blue excitation (λ_{exc} 488 nm) excites selectively the MS form, and is thus able to report even very small mechanochromic effects.

We use software-controlled nanolithography in contact mode to write information with sub-micrometer resolution (**Figure 5**). A seven-letter long word ("Mechano" or "Chromic") is written with high resolution, with each line composing the letters featuring full width at half maximum (FWHM) in the range 400–700 nm, approaching the diffraction limit of confocal detection with a numerical aperture (NA) 1.3 objective (Figure 5c,d). The high color contrast allows for easy detection and reading of the stored information, as apparent from the real-color coded confocal spectral images in Figure 5. Similarly to static vs. dynamic mechanical stresses discussed above, shear stress plays a key-role also in AFM nanolithography. At low writing speed (<10 µm s^{-1}, Figure 5a) the ribbons are engraved with shallow trenches and the resulting information is detectable and clearly distinguished from the cyan background. When the speed is increased to maximally 100 µm s^{-1}, upon the same applied force (24 µN), deeper trenches are engraved, yielding more intense signal but also scattered debris which undermines the readability of the stored information (Figure 5b and movie M2 in the Supporting Information).

Finally, the ribbons are responsive not only to mechanical stresses, but also to light stimuli. Photoconversion of native N form occurs indeed upon excitation with UV or blue light: by using focused laser excitation (405 nm or 473 nm) in a confocal microscope setup, prolonged irradiation results in photo-conversion of the native blue emitting ribbons into yellow emitting ribbons (photoconverted (PC) form). The latter show a very similar luminescence spectrum as the mechanically stressed form. Despite the lack of local information on
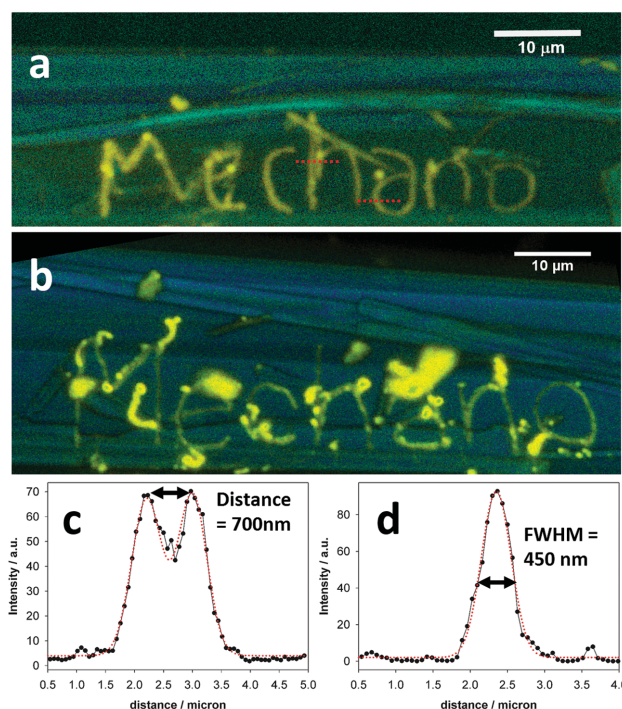

Figure 5. Nanolithography on ultralong ribbons. Confocal spectral images of ribbons engraved with a seven-letter long word ("Mechano") by means of AFM nanolithography conducted at a)10 or (b) 100 µm s^{-1} maximum scan rate, with constant force = 24 µN. Excitation wavelength, emission spectral window, and objective used are 488 nm, 490–700 nm, 63× NA 1.3, respectively. c,d) Intensity profiles of yellow emission across written letters showing the spatial resolution of data storage. Peak-to-peak distance of adjacent resolved lines (d, profile taken from letter "h" across dashed red line in panel (a)) and FWHM of a single line (c, profile from letter "a" of the word "Mechano" across dashed red line in panel (a)). Black lines and dots denote the experimental intensity profiles, red dotted lines are Gaussian fits.

the crystalline structure, the similarity of the photophysical properties between PC and MS forms indicates a substantial analogy between the transformations taking place within the microcrystalline ribbons upon energy feeding by either light or mechanical stimuli. In addition, photostimulation allows to simultaneously deliver energy to the system and to monitor its state, in real time and real space, with high resolution. In particular, we monitored the state of aggregation of complex **1** through continuous acquisition of emission spectra by irradiating at 473 nm, an excitation wavelength which ensures low irradiation intensity of the native ribbons N (which only display a residual absorbance at 473nm) and that maximizes the signal of the developing yellow-emitting PC state. After normalization, the emission spectra—plotted in **Figure 6**a—reveal that photoconversion is a continuous, gradual process, which causes a progressive bathochromic shift of the emission until a final state (PC) is reached, with a similar (although somewhat broader) emission spectrum as MS. The comparison of the intermediate spectra with a linear combination of first and last spectra clearly shows that photoconversion proceeds through several intermediate species, similarly to what also observed for mechanical stimulation (see Figures SI6 and SI7 in the Supporting Information).
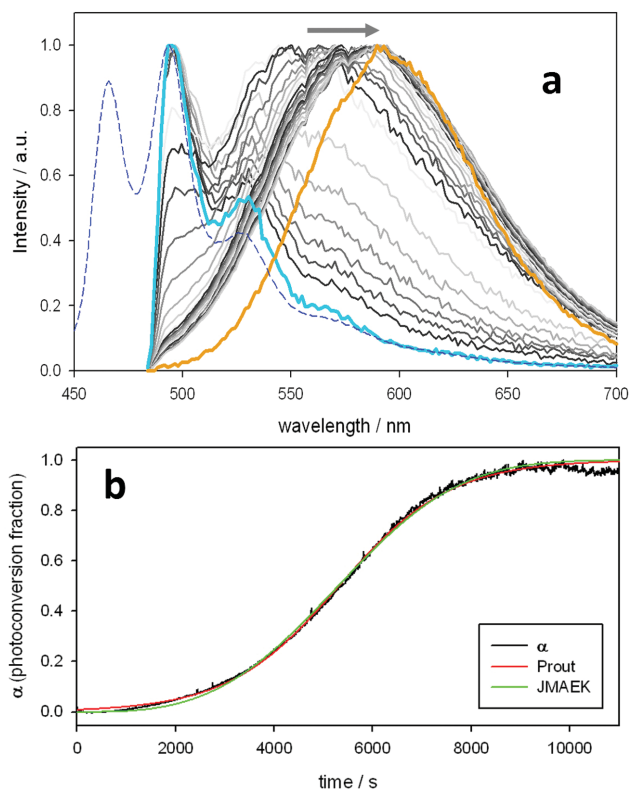
Figure 6. Photoconversion of ribbons luminescence color. a) Emission spectra of N (cyan line), MS (orange line), and during photoconversion of N into PC (gray intensity lines, shifting bathochromically), under continuous irradiation at 473 nm, at low power (500 nW, objective NA 1.3). Spectra were taken with a high-resolution spectrometer in a confocal setup, $\lambda_{exc} = 473$ nm and emission filter cutoff at 485 nm. An emission spectrum of N in a fluorimeter (dashed blue line, $\lambda_{exc} = 375$ nm) is also plotted for comparison. b) Photoconversion fraction kinetic curve, obtained by normalized luminescence in the range 600–620 nm, $\alpha(t) = [I(t) - I(0)]/[I(\infty) - I(0)]$. Emission spectra were taken during photostimulation at irradiation intensity 190 µW. Experimental curves (black) are satisfactorily fitted with two models for autocatalytic solid state reactions, i.e., the Prout–Trompson (red line) and the JMAEK (green line) models.

An accurate analysis of the evolution of the yellow emission signal provides useful insight on the kinetic mechanism of the photoconversion.[15] Even though a detailed discussion on the mechanism is beyond the scope of this paper, we report that the trend of the onset of yellow emission during photoreaction shows satisfactory matching with two different sigmoidal models for solid state kinetics, which have been used to describe autocatalytic reactions, i.e., the Prout–Tompkins and the Johnson–Mehl–Avrami–Erofe'ev–Kolmogorov(JMAEK) models (Figure 6b).[16] Microcrystalline ribbons indeed display different local energies along their structures, arising from defects due to impurities, surfaces, edges, dislocations, cracks, and point defects. At such imperfections the reaction activation energy is minimized, hence they are sites for reaction nucleation where photoconversion likely starts to produce different molecular arrangements than the one of native ribbons N, and in such new arrangements adjacent Pt(II) atoms can interact more closely. The observation of kinetics involving an autocatalytic model indicates that nuclei growth—i.e., photoconversion

evolving from imperfections of the ribbons—promotes formation of new imperfections such as dislocations or cracks at the reaction interface. The inversion point and the final plateau of the sigmoidal shape result from the termination step, which occurs when the fusion of reaction nuclei becomes more probable than branching, i.e., when a large part of the material has photoreacted.

Photoconversion is particularly efficient at relatively low irradiation rates, since at high excitation power other deactivation paths leading to photodegradation of Pt(II) complexes prevail over photoconversion. The prolonged exposure time needed to reach the maximum photoconversion efficiency (several hours), together with the low irradiation power (<1 µW), suggests that photo-conversion relies on a purely photoassisted mechanism and does not involve heat, which is instead dissipated within much a shorter time. This is also supported by the observation that ribbons exposed to conventional heat sources (oven or hot plates at 100 °C) do not undergo any observable photophysical or morphological transformation.

Photoconversion can be conveniently used to locally erase information which has been written with mechanical nano-lithography. We chose to test a ribbon with information written at high speed (100 µm s⁻¹ maximum scan rate) in order to have the highest possible MS signal to be deleted. The high MS signal is due both to deep trenches and to strongly luminescent debris. **Figure 7** shows a written region of a ribbon which, starting from blue-yellow contrast owing to N and MS forms, turns completely to a yellow luminescent form (PC or MS) within 2 h upon exposure to a focused 405 nm laser source. The zoomed out bottom image in Figure 7 reveals that the photoconversion only occurs locally, within the irradiation rectangle, and confirms that information written therein with AFM tip cannot be distinguished anymore after photoconversion. Hence, the information written by mechanical nano-lithography is efficiently hidden and no longer readable, unless high-resolution spectral detection and analysis are performed to retrieve extremely low spectral differences, which are currently beyond the standard resolution of confocal spectral imaging. Such minimal spectral differences could in principle be exploited for application in steganography, a technique based on hiding relevant information behind other, nonrelevant information, while only retrievable with a specific key, i.e., a specific spectral fingerprint.

5. Conclusions

In this contribution we have shown that ultralong ribbons, obtained by the self-assembly of Pt(II) complexes in the absence of Pt···Pt interactions, display high-contrast photoluminescence tribo- and piezochromism. Owing to their excellent flatness and homogeneity in the tens of micrometers scale, the self-assembled ribbons are perfect candidates for nanoscale investigations and for application as individual microsystems for data storage and security.

We have investigated with an AFM tip the mechanochromic response as arising from simple pressure (piezochromism) or friction (tribochromism) on individual ribbons. Moreover, we found that the mechanochromic response is highly localized:
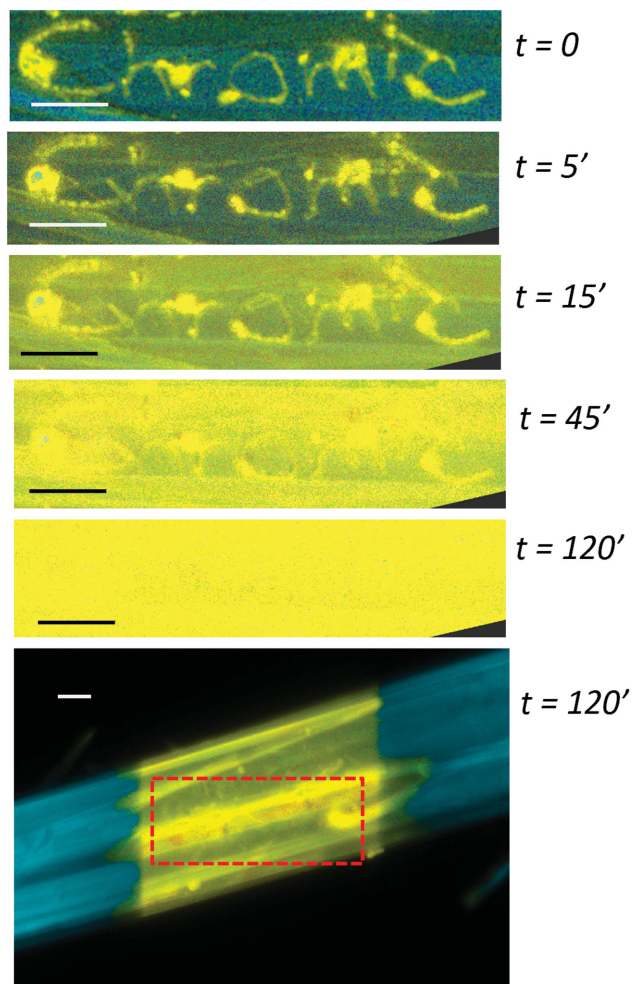
Figure 7. Photoconversion of ribbon luminescence color used to hide information written with AFM nanolithography (seven-letter long word "Chromic" was written at 100 µm s⁻¹ maximum scan rate). Local irradiation at 405 nm is performed on a 50 × 70 µm rectangle including the written information, with a 63× NA 1.3 objective, at nominal power 1 mW. The blue versus yellow contrast of the written information clearly fades during irradiation, and the word "Chromic" is not readable anymore after 2 h irradiation. Excitation wavelength used for imaging is 488 nm, emission spectral window is 490–700 nm and objective used is 63× NA 1.3. The zoomed out image at the bottom, taken with a lower acquisition time and thus not saturated by the strong yellow emission, reveals that the photoconversion only occurs locally within the irradiation area, and confirms that the information is securely erased. For all images, scale bars denote 10 µm.

no propagation of mechanochromism was ever observed in the ribbons.

Following these observations, we proved that mechanochromism can be used to leave luminescent traces of mechanical stress with high fidelity, conserving the spatial resolution of the stressing agent. The tip of an AFM was thus used to write sub-micrometer features on individual ribbons, which are hence used as single memory substrates.

Finally, the ribbons are also responsive to photostimulation: UV light converts the blue-emitting N form of the ribbon into a yellow-emitting form (PC), featuring very similar luminescence

as to that of the mechanically stressed form MS. Therefore, light reduces and eventually cancels out the luminescence contrast between written and unwritten regions of the ribbon. Information written by AFM can thus be securely erased by means of irradiation.

Supporting Information

Supporting Information is available from the Wiley Online Library or from the author.

Acknowledgements

[1] a) Y. Sagara, T. Kato, *Nat. Chem.* **2009**, *1*, 605; b) S. J. Choi, J. Kuwabara, Y. Nishimura, T. Arai, T. Kanbara, *Chem. Lett.* **2012**, *41*, 65; c) X.-P. Zhang, J.-F. Mei, J.-C. Lai, C.-H. Li, X.-Z. You, *J. Mater. Chem. C* **2015**, *3*, 2350.

[2] a) H. H. Pham, I. Gourevich, J. K. Oh, J. E. N. Jonkman, E. Kumacheva, *Adv. Mater.* **2004**, *16*, 516; b) X. Zhu, R. Liu, Y. Li, H. Huang, Q. Wang, D. Wang, X. Zhu, S. Liu, H. Zhu, *Chem. Commun.* **2014**, *50*, 12951; c) T. Aotake, M. Suzuki, K. Tahara, D. Kuzuhara, N. Aratani, N. Tamai, H. Yamada, *Chem. - Eur. J.* **2015**, *21*, 4966.

[3] a) S. Hirata, T. Watanabe, *Adv. Mater.* **2006**, *18*, 2725; b) S.-J. Lim, B.-K. An, S. D. Jung, M.-A. Chung, S. Y. Park, *Angew. Chem., Int. Ed.* **2004**, *43*, 6346; c) C. E. Olson, M. J. R. Previte, J. T. Fourkas, *Nat. Mater.* **2002**, *1*, 225; d) A. Kishimura, T. Yamashita, K. Yamaguchi, T. Aida, *Nat. Mater.* **2005**, *4*, 546.

[4] A. Aliprandi, D. Genovese, M. Mauro, L. De Cola, *Chem. Lett.* **2015**, *44*, 1152.

[5] a) J. R. Kumpfer, S. D. Taylor, W. B. Connick, S. J. Rowan, *J. Mater. Chem.* **2012**, *22*, 14196; b) X. Zhang, J.-Y. Wang, J. Ni, L.-Y. Zhang, Z.-N. Chen, *Inorg. Chem.* **2012**, *51*, 5569.

[6] A. Aliprandi, M. Mauro, L. De Cola, *Nat. Chem.* **2016**, *8*, 10.

[7] J. A. G. Williams, in *Photochemistry and Photophysics of Coordination Compounds II*, 281 (Eds: V. Balzani, S. Campagna), Springer, Berlin **2007**, 205.

[8] a) T. Ohba, A. Kobayashi, H.-C. Chang, M. Kato, *Dalton Trans.* **2013**, *42*, 5514; b) A. Han, P. Du, Z. Sun, H. Wu, H. Jia, R. Zhang, Z. Liang, R. Cao, R. Eisenberg, *Inorg. Chem.* **2014**, *53*, 3338.

[9] G. Wald, *Science* **1964**, *145*, 1007.

[10] a) Q. Benito, B. Baptiste, A. Polian, L. Delbes, L. Martinelli, T. Gacoin, J.-P. Boilot, S. Perruchas, *Inorg. Chem.* **2015**, *54*, 9821; b) Z. Chen, Z. Li, L. Yang, J. Liang, J. Yin, G.-A. Yu, S. H. Liu, *Dyes Pigm.* **2015**, *121*, 170; c) C. Cuerva, J. A. Campo, M. Cano, B. Arredondo, B. Romero, E. Oton, J. M. Oton, *New J. Chem.* **2015**, *39*, 8467; d) J. Forniés, N. Giménez, S. Ibáñez, E. Lalinde, A. Martín, M. T. Moreno, *Inorg. Chem.* **2015**, *54*, 4351; e) Y. Han, H.-T. Cao,

H.-Z. Sun, G.-G. Shan, Y. Wu, Z.-M. Su, Y. Liao, *J. Mater. Chem. C* **2015**, *3*, 2341; f) T. Seki, T. Ozaki, T. Okura, K. Asakura, A. Sakon, H. Uekusa, H. Ito, *Chem. Sci.* **2015**, *6*, 2187; g) Z. Wu, J. Liu, Y. Gao, H. Liu, T. Li, H. Zou, Z. Wang, K. Zhang, Y. Wang, H. Zhang, B. Yang, *J. Am. Chem. Soc.* **2015**, *137*, 12906; h) C. Jobbágy, A. Deák, *Eur. J. Inorg. Chem.* **2014**, *2014*, 4434; i) J. Ni, Y.-G. Wang, H.-H. Wang, Y.-Z. Pan, L. Xu, Y.-Q. Zhao, X.-Y. Liu, J.-J. Zhang, *Eur. J. Inorg. Chem.* **2014**, *2014*, 986.

[11] a) L. Wang, K. Wang, B. Zou, K. Ye, H. Zhang, Y. Wang, *Adv. Mater.* **2015**, *27*, 2918; b) X. Wang, Q. Liu, H. Yan, Z. Liu, M. Yao, Q. Zhang, S. Gong, W. He, *Chem. Commun.* **2015**, *51*, 7497; c) K. Nagura, S. Saito, H. Yusa, H. Yamawaki, H. Fujihisa, H. Sato, Y. Shimoikeda, S. Yamaguchi, *J. Am. Chem. Soc.* **2013**, *135*, 10322; d) J. Wu, H. Wang, S. Xu, W. Xu, *J. Phys. Chem. A* **2015**, *119*, 1303; e) Q. Qi, J. Qian, X. Tan, J. Zhang, L. Wang, B. Xu, B. Zou, W. Tian, *Adv. Funct. Mater.* **2015**, *25*, 4005.

[12] P. Bamfield, *Chromic Phenomena: Technological Applications of Colour Chemistry*, 2nd ed., Royal Society of Chemistry, Cambridge, UK, **2010**.

[13] a) M. Liu, N. A. Amro, G.-Y. Liu, *Annu. Rev. Phys. Chem.* **2008**, *59*, 367; b) G. R. Luis, L. Jian, *J. Phys.: Condens. Matter* **2009**, *21*, 483001.

[14] a) M. Hirtz, M. K. Brinks, S. Miele, A. Studer, H. Fuchs, L. Chi, *Small* **2009**, *5*, 919; b) L. Li, M. Hirtz, W. Wang, C. Du, H. Fuchs, L. Chi, *Adv. Mater.* **2010**, *22*, 1374; c) T. Gan, X. Zhou, C. Ma, X. Liu, Z. Xie, G. Zhang, Z. Zheng, *Small* **2013**, *9*, 2851.

[15] a) K. Užarević, I. Halasz, T. Friščić, *J. Phys. Chem. Lett.* **2015**, *6*, 4129; b) T. Salzillo, S. Zaccheroni, R. G. Della Valle, E. Venuti, A. Brillante, *J. Phys. Chem. C* **2014**, *118*, 9628.

[16] a) A. Khawam, D. R. Flanagan, *J. Phys. Chem. B* **2006**, *110*, 17315; b) E. G. Prout, F. C. Tompkins, *Trans. Faraday Soc.* **1944**, *40*, 488; c) M. Frenette, G. Cosa, T. Friscic, *CrystEngComm* **2013**, *15*, 5100.